

## Nonlinear Law Spectral Technique to Analyze White Spot Syndrome Virus Infection

Mario Alonso Bueno-Ibarra  
Departamento de Biotecnología Agrícola,  
Centro Interdisciplinario de Investigación para el  
Desarrollo Integral Regional (CIIDIR - Sinaloa).  
Blvd. Juan de Dios Bátiz Paredes #250,  
Col. San Juachín,  
Guasave, Sinaloa C.P. 81101.  
[mbueno@ipn.mx](mailto:mbueno@ipn.mx)

María Cristina Chávez-Sánchez  
Laboratorio de Histología,  
Centro de Investigación en Alimentación y Desarrollo  
A.C. (CIAD - Mazatlán).

Av. Sábalo-Cerritos S/N, Estero del Yugo,  
Mazatlán, Sinaloa, México, C.P. 82000.  
[marcris@ciad.mx](mailto:marcris@ciad.mx)

Josué Álvarez-Borrego  
División de Física Aplicada, Departamento de Óptica,  
Centro de Investigación Científica y de Educación  
Superior de Ensenada (CICESE).  
Carretera Ensenada-Tijuana No. 3918,  
Fraccionamiento Zona Playitas.  
Ensenada, Baja California, México, C.P. 22860.  
[josue@cicese.mx](mailto:josue@cicese.mx)

**Abstract** - In this paper a novel spectral technique based on K-Law Fourier nonlinear methodology is developed to classify White Spot Syndrome Virus inclusion bodies found in images from infected shrimp tissue samples. Shrimp culture is expanding in the world due to their high demand and price. This rapid increase in cultured shrimp production was achieved by geographical expansion and technological advances in reproduction in captivity of the white shrimp *Penaeus vannamei*, larval rearing, artificial diet and intensification in growth out systems. However, diseases are one of the major constraints for the sustainable increase of shrimp production. The white spot syndrome virus is a pandemic disease where frequently 100% mortality may occur within 2-3 days. However, several techniques have been implemented and developed for viral and bacterial analysis and diagnostic's tasks; histology is still considered the common tool in medical and veterinary fields. The slide images were acquired by a computational image capture system and a new spectral technique by the development of a spectral index is done to obtain a quantitative measurement of the complexity pattern found in White Spot Syndrome Virus inclusion bodies. After analysis the results show that inclusion bodies are well defined in a clear numerical fringe, obtained by the calculation of this spectral signature index.

**Keywords** - WSSV; image processing techniques; inclusion bodies; shrimp; virus

### I. INTRODUCTION

Several techniques and methods including microscopic observation under light, dark field, phase contrast microscope, bioassay, transmission electron microscopy, immunological, molecular and histopathological methods have been developed for viral and bacterial penaeid shrimps diagnostics [1][2]; these can be divided in traditional morphological pathology, bioassay, microbiology and serology and molecular methods such as PCR, however

histology is still considered the common tool in medical and veterinary for research and diagnostics tasks [3][4][5]. The contribution of aquaculture to world supply of fish, crustaceans, mollusks and other aquatic animals has continued to grow, and has gone from a 3.9% of total production in weight in 1970 to 36.0% in 2006. The world's supply of crustaceans by aquaculture has grown rapidly in the last decade, and has reached 42% of the world production in 2006 and, in that same year, provided the 70% of shrimps and prawns (peneidos) produced worldwide [6]. *Penaeus vannamei* is the most important shrimp species in terms of aquaculture production and is naturally present along the Pacific coast of Central and South America [7].

This species was originally cultured in North, Central and South American countries but at the end of the 1970s, this species was introduced in Asia [8]. In spite of this important increase of shrimp production, the shrimp culture industry has been affected since the 80's with different important diseases [4], being the viruses the most significant pathogens in shrimp. Viral diseases have caused considerable losses of production and jobs, reduced earning, export restrictions, failure and closing of business and decreased confidence of consumers [9].

The white spot syndrome virus (WSSV) is considered as a serious pathogen and is actually a pandemic disease causing important effects in production in many countries with the consequent social impact of many Asian and American countries. México traditionally is considered a privilege country where extensive commercial shrimp aquaculture can be exploited, due its weather and location close to the biggest consumer of the world, United States of America.

Since 2000, in México, shrimp producers from the Northwest of the country have been affected by WSSV. Sinaloa and Nayarit states for example, were reflected their

losses by the reduction of exportations from 30.1 million USD in 2000 compared to the 44.8 million USD in 1999, the losses amount were approximately 14.7 million USD just in one production year, thus producers after this year have been taking actions to control the WSSV disease to reduce their impact [10].

Today the virus continues affecting the production causing the closure of many businesses and affecting the capital of many investors. It is reported by example that in the first half of 2009, the virus has caused mortalities of 70-80 per cent in affected farms in Sinaloa and in Sonora the virus was dispersed in 2008 to areas of the state that had remained free of the pathogen (Personal communication with the Aquatic Health Committees of Sinaloa and Sonora).

WSSV infections have been detected in various tissues and organs, hemolymph, gills, stomach and body cuticular epithelium, hematopoietic tissues, lymphoid organ, antennal glands, connective tissues, muscle tissues, hepatopancreas, heart, midgut, hindgut, nervous tissues, compound eyes, eye, testes and ovaries of naturally and experimentally infected shrimp [11]. WSSV can spread and infect shrimps of any stage of grow-out, asymptotically affecting all life cycle stages, from eggs to broodstock. Once the clinical signs are developed, mortality can reach 100% in 3 days. The causative agent of the disease is an ovoid or ellipsoid bacilliform in shape double-stranded DNA virus (120-150 nm in diameter and 270-290 nm in length), which genus is *Whispovirus*, within the family *Nimaviridae* [12][13].

There is no efficient approach to control this disease, thus, the need for rapid, sensitive diagnostic methods led to develop new alternative techniques in different fields of knowledge. The selection of a method is dependent on the purpose, e.g., histopathology is used to determine the affected organs, the levels of affectation, the pathological changes in cells, tissues and organs and computing optic disciplines can be of support to these conventional methods. Histology makes possible to analyze pathological changes in several tissue cells and allow the pathogen identification, which are sometimes difficult to recognize with other alternative techniques.

For this kind of analysis the method involves several steps to obtain the final sample, which contains a shrimp tissue slice where the inspection is conducted; this tissue slice has a thickness of 1-5  $\mu\text{m}$ , stained with hematoxylin - eosin necessarily to make the examination under microscope. WSSV infection is commonly seen in cuticular epithelial cells and connective tissue cells of the stomach, carapace and gills. However it is also seen in antennal gland, lymphoid organ, hematopoietic tissue and phagocytes of the heart, some WSSV samples are shown in Figure 1.

Infected cells typically have hypertrophied (enlarged) nuclei containing a single intranuclear inclusion. Inclusions at the beginning are eosinophilic and sometimes are separated by a clear halo beneath the nuclear membrane; these are known as Cowdry type A inclusions. Later inclusions become lightly to deeply basophilic and fill the entire nucleus [14], as shown in Figure 2.

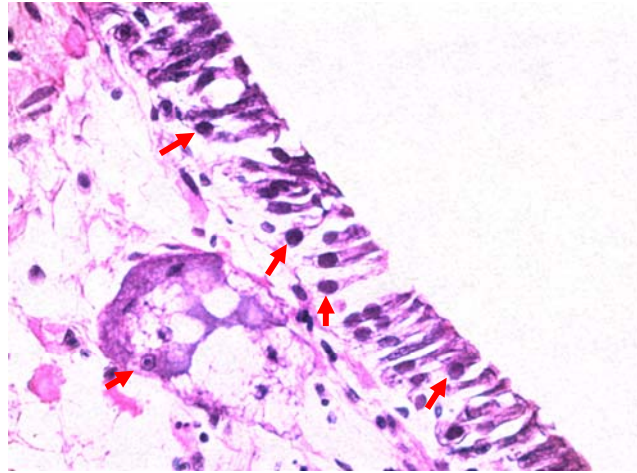


Figure 1. Arrows show samples of connective tissue cells presenting the WSSV infection.

There is no efficient approach to control this disease, however the WSSV early detection can prevent the shrimp's mortality by application of different strategies, one of them may be the RNA genetic technique and it can be constituted as a new therapeutic strategy to control the WSSV infection [15]. Thus, the need for rapid, sensitive diagnostic methods led to develop new alternative techniques in different fields of knowledge like computing optic disciplines that can be of support to conventional methods.

Several optic and computational techniques were developed to recognize these kinds of biological patterns, the analysis of inclusion bodies is determinant of the virus presence, e.g., the color correlation approach used to analyze and recognize the presence of IHHNV inclusion bodies by histological samples from 35 mm transparencies digitalized with a flatbed scanner [16].

The aim of this paper is to extend the development of a new technique to classify the WSSV basophilic and Cowdry type A inclusion bodies, acquired from histological digitalized images from infected shrimps samples by the analysis applied over WSSV sample's slides, based in the application of Fourier spectral filtering techniques, such as K-Law nonlinear filter technique [1].

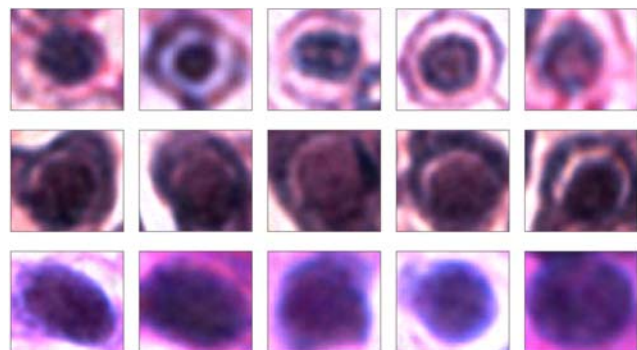


Figure 2. Typical infected shrimp's cells with WSSV basophilic and Cowdry A type inclusion bodies.

These Fourier spectral and color correlation techniques have been demonstrated the capability of analyze important characteristics from viruses and pathogens [16][17][18], including applications in several fields [19][20][21][22].

Therefore, section II describes the core basis of the methodology and the equipment used to obtain the images from infected shrimp tissues; section III presents the results obtained with the spectral signature index developed; additionally the statistical analytic values obtained from this index and the experiments carried out from the digitalized images previously acquired are included; finally in section IV the possible future work that needs to be done to enrich this research is discussed.

## II. MATERIALS AND METHODS

Development of a new technique to analyze and classify WSSV inclusion bodies is divided in five subsections; subsection A describes how the shrimp samples were prepared; subsection B describes the equipment used for image capturing; subsection C describes how had been determined the best spatial color channel function from the multispectral images where the WSSV texture measurement and tissue analysis are carry out by this technique; subsection D explains the mathematical basis used for this technique; finally subsection E describes the steps involved in the obtaining of the classification by the signature index proposed.

### A. Virus sample preparation

Experimental shrimps were obtained from a farm located in the state of Sinaloa, México; transported live to the laboratory to be fixed in Davidson's solution; after 24 h, the fixative was discarded and shrimps were preserved in 50% alcohol solution until they were ready to be processed by conventional histology techniques [2][3][5][13] to obtain the final shrimp tissue histological sample slides, as shown in Figure 3, afterwards they were ready to be examined under microscope.

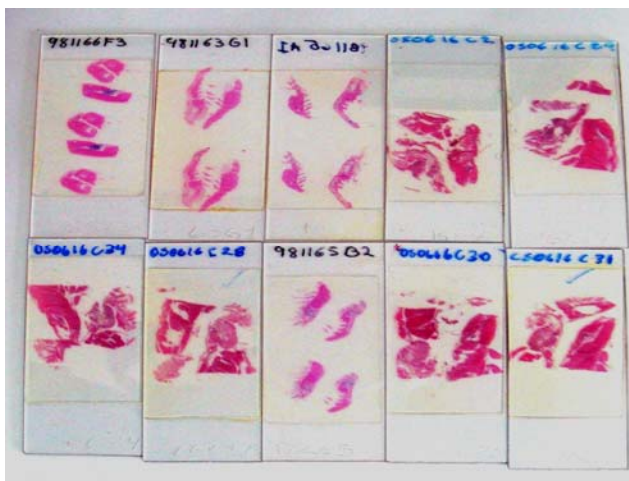


Figure 3. Shrimp tissue histological sample slides ready to be analyzed under microscope.

Several types of WSSV inclusion bodies were selected from cuticular epithelium, connective tissue and abdomen tissue and were digitalized to obtain a filter bank.



Figure 4. Leica microscope model DMRXA2 equipped with a RGB color 3.2 mega pixel digital camera (Leica model DC300) attached to a 2.5 GHz PC Pentium IV.

### B. Digitalized images capture

The WSSV sample slide images were acquired by a novel computational image capture prototype system to enhance the digitalized images with novel autofocus and fusion techniques developed [23][24], running inside a 2.5 GHz PC Pentium 4 with 1 GByte RAM and 80 GBytes HD attached to Leica microscope (model DMRXA2) equipped with a RGB color digital camera (Leica model DC300), as shown in Figure 4.

A set of 168 microscope images were acquired from the shrimp's tissues by 60x objective with a 2088 x 1550 pixels color resolution digital camera; each representative field can contains about an average of 30 to 60 approximately inclusion bodies depending of the level of WSSV infection. Afterwards, a set of 870 WSSV inclusion body images were selected to build a filter bank with 100 most representative WSSV images obtaining the intensity spatial domain matrix data of each WSSV image to be analyzed; thus multispectral function  $f^\lambda(x, y)$  is defined for every pixel coordinates  $x$  and  $y$  on digitalized images, where  $\lambda = \{\lambda_R, \lambda_G, \lambda_B\}$  acquired by a CCD's digital camera with range  $[0, 255]$  and red (R), green (G) and blue (B) are channels in RGB color space representation.

### C. Multispectral analysis for the best spatial function channel determination

Let us introduce some useful definitions and functions:  $f_1^\lambda, f_2^\lambda, f_3^\lambda, \dots, f_w^\lambda$  are a multispectral filter bank of  $W$  captured images of size  $N \times P$  pixels from inclusion body samples taken;  $f_w^\lambda(x, y)$  is the captured image matrix with pixels  $(x, y)$  in the  $w^{\text{th}}$  inside filter bank images, where  $x = 1, \dots, P$ ,  $y = 1, \dots, N$  and  $w = 1, \dots, W$ .

Each inclusion body sample image  $f_w^\lambda(x, y)$  digitalized can be decomposed by their corresponding RGB

$\lambda = \{\lambda_R, \lambda_G, \lambda_B\}$  channels; thus the three intensity matrix data are  $f_w^{\lambda_R}(x, y)$ ,  $f_w^{\lambda_G}(x, y)$  and  $f_w^{\lambda_B}(x, y)$  respectively.

Let  $\hat{H}$  be a vector of real numbers  $\mathbb{R}$ , where  $\hat{H} \in \mathbb{R}$  with  $T$  elements, whose elements are sorted in ascending order with respect to their values, the maximum function  $MAX(\hat{H})$  and the integer function  $\lfloor \eta \rfloor$  of a number can be expressed respectively, like

$$MAX(\hat{H}) = \left\{ h_T \mid h_i \leq h_{i+1}, h_i \in \hat{H}, i = 1, 2, \dots, (T-1) \right\} \quad (1)$$

$$\lfloor \eta \rfloor = \left\{ \delta \mid \delta \in \mathbb{Z}, \eta \in \mathbb{R}, \delta \leq \eta \leq \delta + 1 \right\} \quad (2)$$

where  $\mathbb{Z}$  represent the set of whole numbers.

Every intensity matrix channel of each inclusion body from the filter bank are analyzed by taking a intensity profile vector set  $\{\xi_q^\lambda\}_w$  where  $q = 1, \dots, Q$  vectors and  $\{\xi_q^\lambda\}_w \in f_w^\lambda(x, y)$ , thus  $\{\xi_q^\lambda\}_w$  can be defined by

$$\{\xi_q^\lambda\}_w = f_w^\lambda(x, \zeta_{Vt}), \quad \text{for } Vt = -\lfloor \frac{Q}{2} \rfloor, \dots, \lfloor \frac{Q}{2} \rfloor \quad (3)$$

where  $Vt \in \mathbb{Z}$ ,  $\zeta_{Vt} = \lfloor \frac{N}{2} \rfloor + Vt$  and  $x = 1, \dots, P$ .

Let  $\hat{\Psi}^\lambda$  be a vector of mean values of intensity profile vector set, on each channel, where  $\hat{\Psi}^\lambda \in \mathbb{R}$ , using (3) these mean values can be calculated as

$$\hat{\Psi}_w^\lambda = \frac{\sum_q \{\xi_q^\lambda\}_w}{Q} \quad (4)$$

Figure 5 shows the intensity profile vector set  $\{\xi_q^\lambda\}_w$  graphics calculated from each WSSV channel using (3), afterwards, using (4) can be obtained the pattern measurement of every WSSV channel,  $\hat{\Psi}_w^{\lambda_R}$ ,  $\hat{\Psi}_w^{\lambda_G}$  and  $\hat{\Psi}_w^{\lambda_B}$  respectively. Calculating the maximum value  $MV_\psi$  of the mean values vectors  $\hat{\Psi}^\lambda$  can be obtained the best spatial matrix data from where the WSSV inclusion body pattern is analyzed,  $MV_\psi$  can be obtained by the following expression

$$MV_\psi = MAX \left\{ \hat{\Psi}_w^{\lambda_R}, \hat{\Psi}_w^{\lambda_G}, \hat{\Psi}_w^{\lambda_B} \right\} \quad \text{for } w = 1, \dots, W, \quad (5)$$

therefore the channel source from  $MV_\psi$  has a maximum value indicates the best matrix data, as shown in Figure 6.

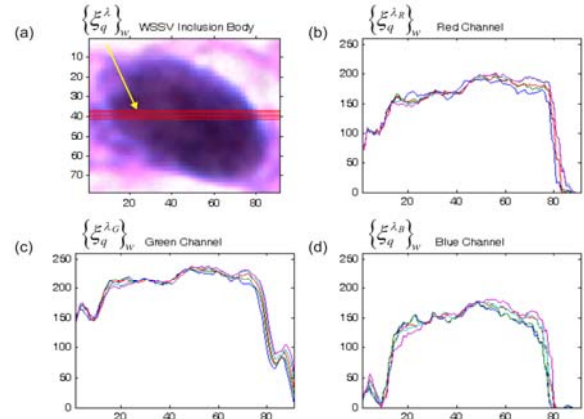


Figure 5. WSSV inclusion body analysis to get the best information channel. (a) intensity vector set, (b) red channel intensity profile, (c) green channel intensity profile and (d) blue channel intensity profile.

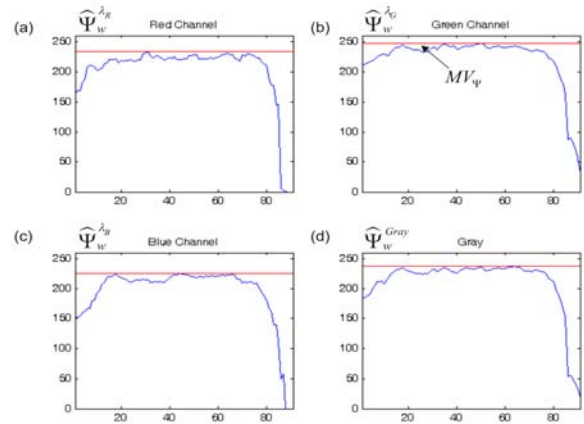


Figure 6. After analyzing the WSSV filter bank and obtaining the maximum value from intensity profile, (a) shows mean values from red channel, (b) shows green channel with the maximum value, (c) shows mean values from blue channel and (d) shows a RGB conversion to gray space with the mean values from its intensity profile.

#### D. WSSV spectral signature index classifier

The spectral signature  $SSF$  can be defined like a function to obtain the spectral properties of  $f_w^\lambda(x, y)$  from a specific RGB channels  $\{\lambda_R, \lambda_G, \lambda_B\}$ ; whereas the spectral signature index  $i^{ss}$  was developed to get a quantitative measurement of the inclusion bodies complexity pattern.

Let  $i^{ss}$  be defined like scalar number valued  $i^{ss} \in \mathfrak{R}^+$  to measure the spectral frequency properties found in  $f_w^\lambda(x, y)$  obtained by  $SSF$  function, let  $I^{\lambda_G}(x, y)$  be the intensity matrix data obtained by  $f_w^\lambda(x, y)$  green channel, where WSSV inclusion bodies characteristics are protruded.

Let function  $I_{Contour}^{\lambda_G}(x, y) \in [0, 1]$  be the WSSV inclusion body contour of the function  $I^{\lambda_G}(x, y)$  calculated by the application of active contour technique (also known as a “snake”) as follows

$$I_{Contour}^{\lambda_G}(x, y) = -|G_{\sigma}(x, y) * \nabla^2 I^{\lambda_G}(x, y)|^2, \quad (6)$$

where  $\nabla^2$  is the Laplacian operator,  $G_{\sigma}(x, y)$  is a Gaussian standard deviation  $\sigma$ , afterwards the edge is obtained by the zero-crossings of  $G_{\sigma}(x, y) * \nabla^2 I^{\lambda_G}(x, y)$  in the Marr-Hildreth theory [25].

Morphological reconstruction has a broad spectrum of several functions, e.g., like those to filling holes, defining the function  $I_{WSSV-Seg}^{\lambda_G}(x, y)$  to be the image segmentation of WSSV inclusion body function  $I^{\lambda_G}(x, y)$ , it can be obtained by filling the area of WSSV inclusion body contour calculated by (6), let  $B_{in} = \{(x, y)\}$  be the pixel coordinates set delimited by the area of the function  $I_{Contour}^{\lambda_G}(x, y)$ , then the pixel coordinates set can be obtained by  $B_{in} = \{(x, y) | inside I_{Contour}^{\lambda_G}(x, y) = 1\}$ , afterwards the general segmentation function  $I_{Seg}^{\lambda_G}(x, y)$  can be defined as follows

$$I_{Seg}^{\lambda_G}(x, y) = \begin{cases} 1 & \{\forall (x, y) | \varphi(x, y) \in \gamma_{in}\} \\ 0 & otherwise \end{cases}, \quad (7)$$

where  $I_{WSSV-Seg}^{\lambda_G}(x, y) = I_{Seg}^{\lambda_G}(x, y)$ ,  $\varphi(x, y) = I_{Contour}^{\lambda_G}(x, y)$  and  $\gamma_{in} = B_{in}$ .

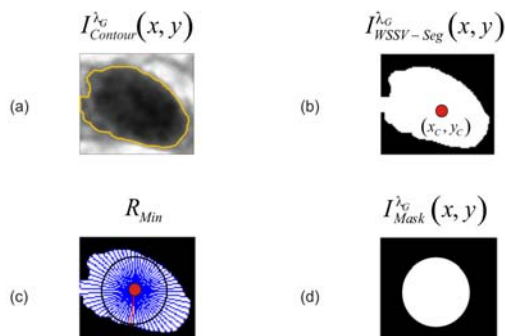


Figure 7. Segmentation steps, (a) shows the contour from WSSV inclusion body, (b) shows the centroid coordinates and image segmentation, (c) shows the calculation of minimum radius and (d) shows the circular mask to apply into its WSSV pattern analysis.

Once WSSV inclusion body segmented function is obtained, it is necessarily to make the analysis just inside of the WSSV inclusion body pattern, thus a binary circular

function  $I_{Mask}^{\lambda_G}(x, y)$  is calculated inside the segmented function  $I_{Seg}^{\lambda_G}(x, y)$ .

The center of the circular mask function is calculated by obtaining the centroid  $(x_c, y_c)$  of the WSSV inclusion body segmentation  $I_{WSSV-Seg}^{\lambda_G}(x, y)$ , the coordinates  $(x_c, y_c)$  can be calculated by the following pair equations as

$$x_c = \frac{\sum_{i=1}^P \sum_{j=1}^N (i) * I_{WSSV-Seg}^{\lambda_G}(i, j)}{\sum_{i=1}^P \sum_{j=1}^N I_{WSSV-Seg}^{\lambda_G}(i, j)} \quad (8)$$

and

$$y_c = \frac{\sum_{i=1}^P \sum_{j=1}^N (j) * I_{WSSV-Seg}^{\lambda_G}(i, j)}{\sum_{i=1}^P \sum_{j=1}^N I_{WSSV-Seg}^{\lambda_G}(i, j)}. \quad (9)$$

The minimum radius  $R_{Min}$  of the circular binary mask where the WSSV inclusion body pattern will be analyzed centered on  $(x_c, y_c)$ , can be obtained defining the function  $R(\theta)$  used to calculate the magnitude of a vector beginning in coordinates  $(x_c, y_c)$  until reach the edge of  $I_{WSSV-Seg}^{\lambda_G}(x, y)$  in  $\theta$  direction as follows

$$R(\theta) = \left\{ \begin{array}{l} r | x^* = r \cdot \cos(\theta); y^* = r \cdot \sin(\theta) \\ | r = r + 1 : r \in \mathbb{Z}^+ \text{ if } I_{WSSV-Seg}^{\lambda_G}(x_c + x^*, y_c + y^*) = 1 \end{array} \right\}. \quad (10)$$

Afterwards doing  $r_1 = R(\theta)$  and  $r_2 = R(\theta + \Delta\theta)$  where a counterclockwise angle increment is  $\Delta\theta$ , thus the minimum radius  $R_{Min}$  can be defined by

$$R_{Min} = \left\{ \begin{array}{l} r_1 \text{ if } r_1 \leq r_2 \\ r_2 \text{ otherwise} \end{array} \right\}, \quad (11)$$

then using (10) and (11) for  $\theta = 0, \dots, 2\pi - \Delta\theta$  is obtained  $R_{Min}$ . Let the function  $Circ(R_{Min})$  be the circle created by the rotation of  $R_{Min}$ , then the  $I_{Mask}^{\lambda_G}(x, y)$  circular binary mask function using (7) is obtained by  $I_{Mask}^{\lambda_G}(x, y) = I_{Seg}^{\lambda_G}(x, y)$  doing  $\varphi(x, y) = Circ(R_{Min})$  and  $\gamma_{in} = \{(x, y) | inside Circ(R_{Min}) = 1\}$ , as shown in Figure 7.

Let the function  $I_{IB}^{\lambda_G}(x, y)$  be the intensity matrix data resulted after the application of the  $I_{Mask}^{\lambda_G}(x, y)$  circular binary mask function over the area where inclusion bodies are analyzed; thus  $I_{IB}^{\lambda_G}(x, y) = I^{\lambda_G}(x, y) \Delta I_{Mask}^{\lambda_G}(x, y)$ , where  $\Delta$  represents the bitwise multiplication.

Let us  $A_{Mask}$  be defined such as the circular binary mask's total area over the region of interest analyzed of the inclusion bodies, defined by

$$A_{Mask} = \sum_{x,y} I_{Mask}^{\lambda_G}(x, y), \text{ for } I_{Mask}^{\lambda_G}(x, y) > 0. \quad (12)$$

K-Law nonlinear filter function (K-Law) in pattern recognition is used to analyze and explore the discriminating property quality of each filter [26] over the WSSV inclusion body segmented image  $I_{IB}^{\lambda_G}(x, y)$  function.

K-Law filter function is derived by the Fourier transform of the  $I_{IB}^{\lambda_G}(x, y)$  function, denoted by

$$I_{IB}^{\lambda_G}(u, v) = |I_{IB}^{\lambda_G}(u, v)|^k \exp[-i\phi(u, v)], \quad k = 1. \quad (13)$$

The K-Law nonlinear filter of  $I_{IB}^{\lambda_G}(x, y)$  is applied by the change of value  $0 < k < 1$  in (13), where  $k$  is the nonlinear strength; thus intermediate values of  $k$  permit the variability of filter features [27].

Let  $f_w^{\lambda_G}(u, v)$  function be defined by the application of K-Law Fourier related filter, calculated over the  $I_{IB}^{\lambda_G}(x, y)$

denoted by

$$f_w^{\lambda_G}(u, v)_k = I_{K-Law}^{\lambda_G}(u, v)_w, \quad 0 < k < 1 \quad (14)$$

where  $k = 0.1$  is used in (13) and  $u, v$  are variables in frequency domain.

The *SSF* function can be obtained by

$$SSF(f_w^{\lambda_G}(u, v)_k) = \begin{cases} 1, & \text{if } \text{Re}(f_w^{\lambda_G}(u, v)_k) > 0 \\ 0, & \text{otherwise} \end{cases}, \quad (15)$$

where  $f_w^{\lambda_G}(u, v)_k$  is obtained by (14).

Finally, the spectral signature index  $i^{ss}$  is developed and can be defined by

$$i^{ss} = \left\{ \frac{SSF(f_w^{\lambda_G}(u, v)_k)}{(A_{Mask})_w} \mid (u, v) \in \mathbb{C} \right\}, \quad (16)$$

where *SSF* and  $A_{Mask}$  are obtained respectively according by (15) and (12) for every image  $f_w^{\lambda_G}(x, y)$  found in the inclusion bodies filter bank.

*E. Spectral signature index classifier block diagram*

Figure 8 shows the block diagram of the new spectral technique involved in WSSV inclusion bodies classification by measurement of the spectral signature index  $i^{ss}$  over the infected shrimp's tissue patterns.

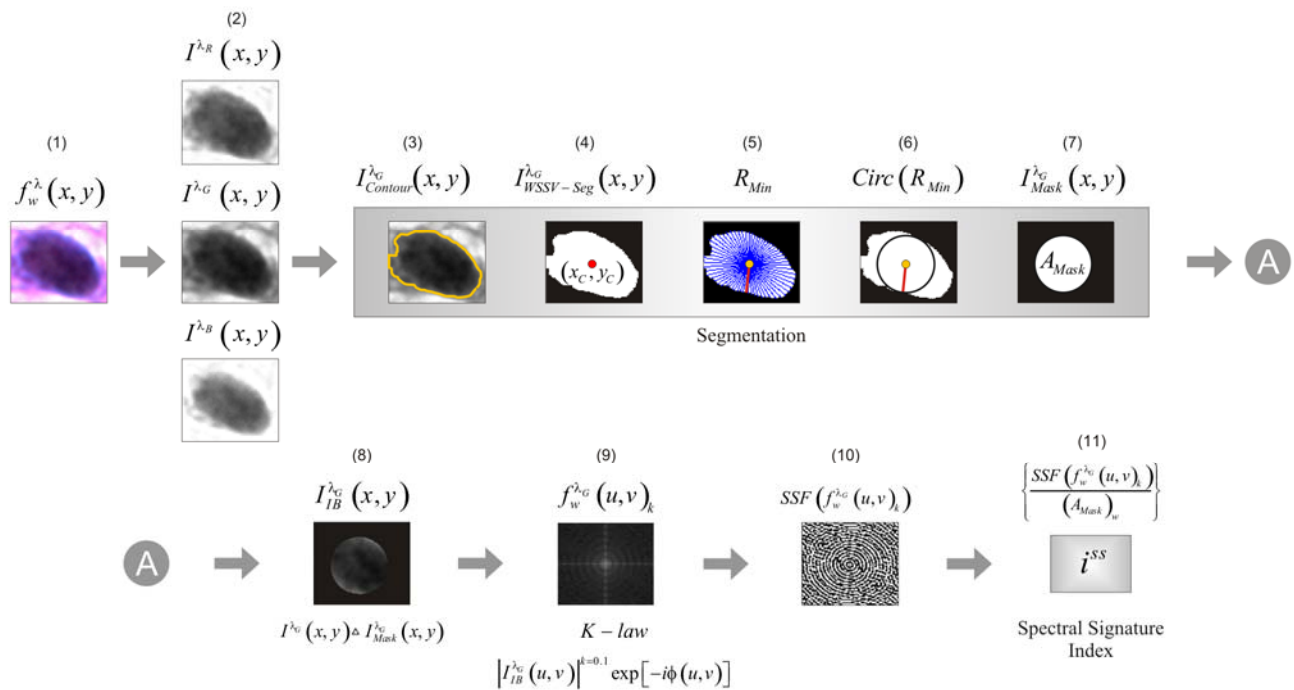


Figure 8. Block diagram to obtain the developed spectral signature index.

This methodology is explained by the following steps: 1) The  $f_w^\lambda(x, y)$  function is acquired from WSSV inclusion bodies color image sample filter bank; 2) This  $f_w^\lambda(x, y)$  is divided into its RGB  $I^{\lambda_r}(x, y)$ ,  $I^{\lambda_g}(x, y)$  and  $I^{\lambda_b}(x, y)$  functions; 3) Segmentation of  $I^{\lambda_g}(x, y)$  by using contour “snake” techniques and a morphological operator to get the function  $I_{Contour}^{\lambda_g}(x, y)$ ; 4) Filling the function  $I_{Contour}^{\lambda_g}(x, y)$  is obtained the function  $I_{WSSV-Seg}^{\lambda_g}(x, y)$ , afterwards is calculated the centroid coordinates  $(x_c, y_c)$  on this function; 5) From centroid coordinates  $(x_c, y_c)$  towards the edge of function  $I_{WSSV-Seg}^{\lambda_g}(x, y)$  is obtained the minimum radius  $R_{Min}$ ; 6) By rotating  $R_{Min}$  centered on  $(x_c, y_c)$  is obtained the function  $Circ(R_{Min})$  used to build the final circular mask; 7) A circular mask function  $I_{Mask}^{\lambda_g}(x, y)$  is created inside  $I_{WSSV-Seg}^{\lambda_g}(x, y)$  by filling the area of the function  $Circ(R_{Min})$ , where WSSV inclusion body pattern is analyzed, at same time the area  $A_{Mask}$  is calculated from the  $I_{Mask}^{\lambda_g}(x, y)$  binary mask function; 8) Using  $I_{Mask}^{\lambda_g}(x, y)$  function, segmentation operation is applied over the WSSV inclusion body area  $I^{\lambda_g}(x, y)$ , where is obtained the  $I_{IB}^{\lambda_g}(x, y)$  function; 9) K-Law nonlinear operation is applied in  $I_{IB}^{\lambda_g}(x, y)$  function to get the  $I_{K-Law}^{\lambda_g}(u, v)_w$  function then it becomes into  $f_w^{\lambda_g}(u, v)_k$  function in frequency domain; 10) The frequencies are extracted and analyzed from  $f_w^{\lambda_g}(u, v)_k$  by the function  $SSF$  and 11) the K-Law spectral signature index  $i^{ss}$  is calculated using (16).

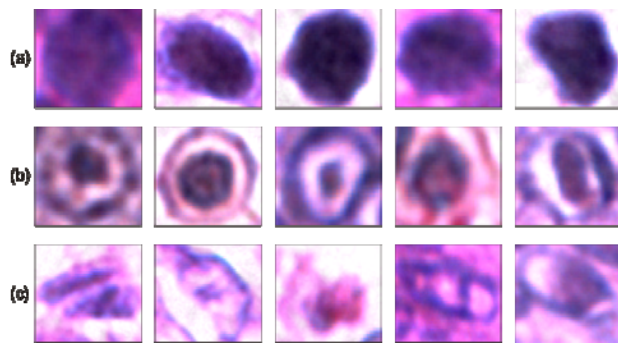


Figure 9. (a) WSSV strong basophilic inclusion bodies, group I; (b) WSSV white halo and chromatin Cowdry type A inclusion bodies, group II; (c) Non-infected tissue particles, group III.

TABLE I. SPECTRAL SIGNATURE INDEX STATISTICAL VALUES

WSSV Group	Signature Index Statistical Behavior			
	$\bar{x}_{i^{ss}}$	$\sigma_{i^{ss}}$	1SE	2SE
I	1.3748	0.4817	0.0852	0.1703
II	2.6069	1.8533	0.4953	0.9906
III <sup>a</sup>	159.4229	352.5394	94.2201	188.4402
IV <sup>b</sup>	1.7498	1.2362	0.1823	0.3645

a. Non-infected tissue group particles;  
b. Groups I and II analyzed together.

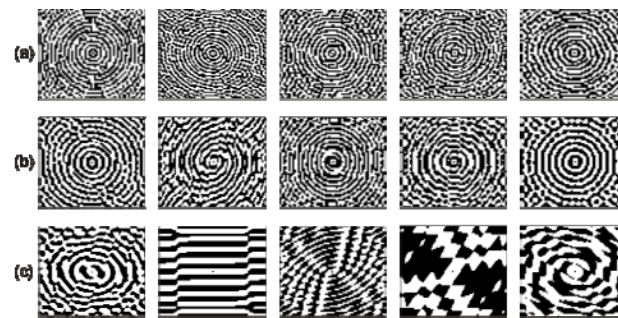


Figure 10. (a) SSF frequencies of group I; (b) SSF frequencies of group II; (c) Non-infected particles SSF frequencies, group III.

### III. RESULTS

In order to see if this technique is working with a good performance with the groups of representative inclusion bodies of WSSV with different morphological images, were analyzed with spectral signature index; their images and an additional group of non-infected tissue particles are shown in Figure 9; hence in Table 1 the statistical behavior values of the spectral signature index are shown, including the mean value  $\pm 2SE$  (two standard errors).

A set of 168 microscope image field samples were acquired without any additional preprocessing like illumination or contrast correction just the fusion technique developed by [24]; then from this set 870 WSSV inclusion body images were cut, selecting 100 most representative WSSV inclusion bodies to build a filter bank, afterwards every WSSV inclusion body pattern were analyzed to get their frequency measurement and addition to build the biogenic particle cluster by this spectral index.

The great difference in the statistical values of the infected particles with the non infected particles is due to the behavior of WSSV inclusion bodies frequencies in the green channel complex plane, while the non-infected cells do not show similar frequency properties, the infected particles show a well determined frequency signature; in Figure 10 are presented some examples of these frequencies behavior. All the WSSV inclusion bodies were analyzed together; the results shows that the complete inclusion bodies group can be located in well defined fringe  $1.3853 \leq i^{ss} \leq 2.1143$  with  $(\pm 2SE)$ .

#### IV. CONCLUSION AND FUTURE WORK

This paper presents a new technique to classify WSSV inclusion bodies from infected shrimp tissue image, based on the analysis of frequencies found in the green channel with K-Law non-linear filter.

Representative groups of WSSV inclusion bodies from infected shrimp tissues and organs were analyzed. The results show that inclusion bodies are well defined in a clear numerical fringe; thus it can be inferred that whatever analyzed particle with a spectral signature index  $i_k^{ss}$  value outside of  $1.3853 \leq i_k^{ss} \leq 2.1143$  range can be considered as non-infected particle.

Future work can be done in the development of automatic WSSV identification system applying this spectral index classifier; however this kind of classifier can be extended by combining complementary frequency analysis techniques by Fourier related filters on the calculation of the spectral signature index to obtain better discriminating results.

Experiments with new tissue samples can be done from others shrimps organs where the virus has a different pattern and its identification is more complex.

Finally, the potential of this signature index can be used to classify other kind of shrimp's viruses and/or other animal, human viruses or biogenic particles.

#### ACKNOWLEDGMENT

This document is based on work partially supported by CONACYT under Grant No. 102007.

#### REFERENCES

- [1] Bueno-Ibarra M. A., Chávez-Sánchez M. C. and Álvarez-Borrego J., "Development of nonlinear k-law spectral signature index to classify white spot syndrome virus basophilic inclusion bodies". The First International Conference on Advances in Bioinformatics and Application (BIOINFO 2010), Cancún, México, March 7-13 2010, pp. 30-33.
- [2] Lightner D. V. and Redman R. M., "Shrimp diseases and current diagnostic methods", *Aquaculture*, vol. 164, Issue 1-4, May 1998, pp. 201-220.
- [3] Lightner D. V., "A handbook on shrimp pathology and diagnostic procedures for diseases of cultured penaeid shrimp", World Aquaculture Society, Baton Rouge, LA, USA, 1996.
- [4] Peinado-Guevara L. I. and López-Meyer M., "Detailed monitoring of white syndrome virus (WSSV) in shrimp commercial ponds in Sinaloa, México by nested PCR", *Aquaculture*, vol. 251, Issue 1, January 2006, pp. 33-45.
- [5] Bell T. A. and Lightner D. V., "A Handbook of Normal Shrimp Histology Special Publication No. 1", World Aquaculture Society, Baton Rouge, LA, USA, 1988, pp. 1-114.
- [6] FAO. The State of World Fisheries and Aquaculture. FAO Fisheries and aquaculture Department. Food and Agriculture Organization of the United States. 2008, p. 196.
- [7] Holthuis, L.B., FAO species catalogue. Shrimps and prawns of the world. An annotated catalogue of species of interest to fisheries. FAO Fish. Synop., (125) vol. 1: 1980, p. 261.
- [8] Briggs M., Funge-Smith S., Subasinghe R. and Philips M., "Introductions and movement of *Penaeus vannamei* and *Penaeus stylirostris* in Asia and the pacific". FAO, Bangkok, 2004, p. 32.
- [9] Bondad-Reantaso M.G., Subasinghe R.P., Arthur J.R., Ogawa K., Chinabut S., Adlard R., Tan Z. and Shariff M., "Disease and health management in Asian" *Aquaculture*. *Vet. Parasitol.* (132), 2005, pp. 249-272.
- [10] Walker Peter J. and Mohan C. V., "Viral disease emergence in shrimp aquaculture: origins, impact and the effectiveness of health management strategies", *Reviews in Aquaculture*, vol. 1, February 2009, pp. 125-154.
- [11] Chávez-Sánchez M. C. and Montoya-Rodríguez Leobardo, "Enfermedades virales, un reto a la camaronicultura", Primer Foro de Pesca y Acuicultura de las Costas de Chiapas, ECOSUR, Unidad Tapachula, Chapter II, September 2001, pp. 17-24.
- [12] OIE. Manual of diagnostic test for aquatic animals. [http://www.oie.int/eng/normes/fmanual/A\\_summry.htm](http://www.oie.int/eng/normes/fmanual/A_summry.htm), 2009.
- [13] Lightner D. V. and Pantoja Carlos R., "A handbook of penaid shrimp diseases and diagnostic methods (English and Spanish versions.)", A publication in cooperation between the University of Arizona and United States Department of Agriculture (USDA-USAID-CSREES), as part of the Hurricane Mitch Reconstruction Program of Central America (Spanish version), 2001, pp. 48-57.
- [14] OIE. Manual of diagnostic test for aquatic animals. [http://www.oie.int/esp/normes/fmanual/A\\_summry.htm](http://www.oie.int/esp/normes/fmanual/A_summry.htm), 2003.
- [15] Xu J., Han F. and Zhang X., "Silencing shrimp white spot syndrome virus (WSSV) genes by siRNA", *Antiviral Research*, vol. 73, Issue 2, Feb 2007, pp. 26-131.
- [16] Álvarez-Borrego J. and Chávez-Sánchez M. C., "Detection of IHNV virus in shrimp tissue by digital color correlation" *Aquaculture*, vol. 194, Issue 1-9, August 2000.
- [17] Álvarez-Borrego J. and Fajer-Ávila Emma J., "Identification of platyhelminth parasites of the wild bullseye pufferfish (*Sphoeroides annulatus*, Jenyns, 1853) using invariant digital color correlation", *Marine Biology and Oceanography México*, vol. 41(1), July 2006, pp. 129-139.
- [18] Mouriño-Pérez Rosa R., Álvarez-Borrego J. and Gallardo-Escárate C., "Digital color correlation for the recognition of *Vibrio cholerae* O1 in laboratory and environmental samples", *Marine Biology and Oceanography México*, vol. 41(1), July 2006, pp. 77-86.
- [19] Coronel-Beltrán A. and Álvarez-Borrego J., "Comparative analysis between different font types and styles letters using a nonlinear invariant digital correlation", *Journal of Modern Optics*, vol. 57(1), January 2010, pp. 58-64.
- [20] González-Fraga J. A., Kober V., Álvarez-Borrego J. and I. A. Ovseevich, "Pattern recognition of fragmented objects with adaptive correlation filters", *Optical Memory & Neural Networks*, vol. 15, No. 3, ISSN 1060-99XX, 2006.
- [21] Millán, M. S., Campos J., Ferreira C., Yzuel M. J., "Matched filter and phase only filter performance in colour image recognition", *Optics Communications*, vol. 73(4), 1989, pp. 277-284.
- [22] Millán, M. S., Yzuel M. J., Campos J., Ferreira C "Different strategies in optical recognition of polychromatic images", *Applied Optics*, vol. 31(14), 1992, pp. 2560-2567.
- [23] Bueno-Ibarra M. A., Álvarez-Borrego J., Acho L. and Chávez-Sánchez M. C., "Fast autofocus algorithm for automated microscopes", *Optical Engineering*, vol. 44(6), 063601-1, 2005.
- [24] Bueno-Ibarra M. A., Álvarez-Borrego J., Acho L. and Chávez-Sánchez M. C., "Polychromatic image fusion algorithm and fusion metric for automatized microscopes", *Optical Engineering*, vol. 44(9), 093201-1, September 2005.
- [25] M. Kass, A. Witkin, and D. Terzopoulos, "Snakes: Active contour models.", *International Journal of Computer Vision*. vol. 1(4), 1987, pp. 321-331.
- [26] González-Fraga J.A., Kober V. and Álvarez-Borrego J., "Adaptive SDF filters for pattern recognition", *Optical Engineering*, vol. 45, 057005, 2006.
- [27] Guerreo-Moreno R. E. and Álvarez-Borrego J., "Nonlinear composite filter performance", *Optical Engineering*, vol. 48(6), 067201-1, June 2009.